

LASER APPLICATIONS AND OTHER TOPICS IN QUANTUM ELECTRONICS PACS numbers: 42.25.Gy; 78.67.Bf; 42.81.Pa
DOI: 10.1070/QE2014v044n10ABEH015418

On the possibility of detecting local refractive index changes in optically transparent objects by means of a point nanoantenna attached to a fibre microaxicon

Yu.N. Kulchin, O.B. Vitrik, A.A. Kuchmizhak

Abstract. **It is shown theoretically that the use of the spectral registration of the dipole local plasmon resonance (DLPR) displacement in a single spherical gold nanoantenna, placed near the surface of a homogeneous dielectric medium, allows the mapping of extremely small variations (to 5×10^{-4}) of the refractive index (RI) of this medium. Using the quasi-static approximation, we have developed an analytic model that allows evaluation of the spectral displacement of the nanoantenna DLPR depending on the variation in the medium refractive index. The point probe based on a fibre microaxicon with a gold spherical nanoantenna attached to its top is proposed that allows practical implementation of the developed RI scanning method. Numerical calculations of the probe characteristics using the time-domain finite-difference method are presented, and it is shown that for the case of a gold spherical nanoantenna of small size, comparable with the skin layer thickness in gold, the relative spectral shift value is in good agreement with the results obtained by using the developed analytic model.**

Keywords: *metallic spherical nanoantenna, local dipole plasmon resonance, refractive index mapping, spectral detection.*

1. Introduction

At present the development and creation of various types of nanodevices and functional elements require high-quality methods for microscopic analysis of their critical dimensions, elemental composition, topographic and local optical properties [1]. Whereas the problem of studying the structural and topographic properties of the objects can be efficiently solved using the methods of atomic force microscopy (AFM) and electron microscopy, the methods of detecting small variations in the refractive index (RI) that characterise the chemical composition and local optical properties of the studied object are usually based on the interaction of the studied object surface with light fields possessing sub-wavelength localisation [2–5].

Yu.N. Kulchin, A.A. Kuchmizhak Institute of Automation and Control Processes, Far Eastern Branch, Russian Academy of Sciences, ul. Radio 5, 690041 Vladivostok, Russia;
e-mail: kulchin@iacp.dvo.ru, alex.iacp.dvo@mail.ru;
O.B. Vitrik Institute of Automation and Control Processes, Far Eastern Branch, Russian Academy of Sciences, ul. Radio 5, 690041 Vladivostok, Russia; Far Eastern Federal University, ul. Sukhanova 8, 690041 Vladivostok, Russia; e-mail: oleg_vitrik@iacp.dvo.ru

Received 25 February 2014; revision received 18 March 2014
Kvantovaya Elektronika **44** (10) 975–980 (2014)
Translated by V.L. Derbov

An obstacle for attaining a high degree of localisation in light radiation interacting with the studied object by means of far-field optical methods is the existence of the fundamental diffraction limit [6]. Essentially higher efficiency in solving the problems of nanoscale optical field concentration and control is demonstrated by nanoantennas [7, 8], making it possible to implement such practical applications as optical manipulation of nanoobjects [8], nanolithography [9], excitation and detection of fluorescence from single molecules with the spatial resolution to 20 nm [10], as well as the super-resolution microscopy of RI variation [11]. In the latter case, in order to provide the possibility of high-precision nanoantenna movement near the surface of the object and the local RI variation mapping, the nanoantenna should the placed at the tip of a scanning probe. In the apertureless near-field scanning optical microscopy (NSOM), the role of the nanoantenna is played by a metallic tip of the AFM cantilever, concentrating the radiation due to the lightning arrester effect [3, 4, 12]. The radiation, concentrated near the tip of the nanoantenna probe, is scattered from the surface of the studied object. The intensity of the scattered signal varies depending on the change in the topographic and local optical properties of the surface [12] or even the subsurface layer of the object [13], providing the possibility of determining its chemical composition by means of the apertuless NSOM method. However, the focal spot exposing the nanotip is rather large, giving rise to the appearance of the background that essentially complicates the useful signal detection. This problem can be solved by detecting the nonlinear response [14] or using the modulation technique of signal selection [15], which significantly complicates the practical implementation of apertuless-NSOM-based high-resolution refractometers. Besides that, in many problems the presence of a large exposure region is extremely undesirable [16].

The problem of background illumination can be avoided by using NSOM probes of the aperture-type NSOM that implement the idea of a point nanoantenna [17]. As a rule, such a nanoantenna is a localised light source, implemented as a nanodimensional aperture at the exit of an optical fibre coated with a nontransparent metallic film [18]. However, the small transmission of the nanodimensional hole essentially restricts both the lateral resolution (to 50–100 nm) and the sensitivity of the apertured NSOM method in the recording of the local RI variations. The use of resonance apertures (butterfly aperture [19], C-aperture [20], apertures surrounded by concentric grooves [21]) with enhanced transmission allows the improvement of the lateral resolution of the apertured NSOM methods (to 20 nm). However, it provides rather low

sensitivity when recording small RI variations (12% intensity change at extremely high variation of the RI by $\Delta n \sim 2$ [21].

It is known that the use of spectral principles of registration in NSOM profilometers instead of the amplitude ones allows an increase in the sensitivity and the signal-to-noise ratio in these systems [22, 23]. It is expected that the implementation of the analogous approach, based on detecting the spectral response of a point nanoantenna rather than the amplitude one, will allow increasing the sensitivity of NSOM methods to small variations of RI. This approach can be based on the pronounced dependence of the position of the dipole local plasmon resonance (DLPR) spectral peak in metallic nanoparticles of different shape on the change in the surrounding medium RI [24]. Therefore, a metallic nanoparticle, placed at the tip of the scanning probe, can play the role of a point nanoantenna, whose spectral response detection will allow high-precision mapping of the RI variations at the surface of the studied object.

In the present paper we demonstrate theoretically for the first time the possibility of detecting extremely small local RI variations (to 5×10^{-4}) by recording the spectral response of the simplest point nanoantenna, a spherical gold nanoparticle placed at the tip of a transparent dielectric probe, implemented as a fibre microaxicon (FMA). We have shown that the use of a fibre axicon as the probe base can provide efficient excitation of DLPR in the nanoantenna being exposed to focused radiation with the focal spot size approaching the diffraction limit. We have also demonstrated the shift of the DLPR spectral position in a spherical nanoantenna, placed near the surface of the studied object. The estimates carried out on the basis of the time-domain finite-difference method for the case when the nanoantenna diameter does not exceed the doubled thickness of the gold nanoantenna skin layer, are in good agreement with the analytic model developed in the present paper on the basis of the quasi-static theory.

2. Theoretical model

To substantiate the possibility of detecting the DLPR spectral position shift in a nanoantenna, placed near the surface of the studied object, we used the quasi-static theory. It is known that the effect of an electromagnetic wave having the electric field strength E on a gold spherical nanoparticle with the radius a and the dielectric constant ε_{Au}, surrounded by a transparent homogeneous dielectric with $\varepsilon = 1$, leads to the polarisation of the particle giving rise to the dipole moment

$$\boldsymbol{p} = 4\pi a^3 \varepsilon_0 \frac{\varepsilon_{Au} - 1}{\varepsilon_{Au} + 2} \boldsymbol{E}, \tag{1}$$

where ε_0 is the electric constant. Below we assume that the nanoparticle centre is separated by the distance $z_0 = d + a$ from the planar boundary of a semi-infinite medium having the permittivity ε_m, and that the electric field of the incident radiation is polarised in the direction, perpendicular to the surface of the medium (s-polarisation, Fig. 1a). In this case; the polarised nanoantenna will induce surface charges in the medium, the field of which can be presented as the field of the equivalent reflected dipole [12, 25] with the dipole moment $\boldsymbol{p}_{ekv} = \alpha \boldsymbol{p}$, $\alpha = (\varepsilon_m - 1)/(\varepsilon_m + 1)$, located inside the medium at the distance $2z_0$ from the nanoparticle centre (Fig. 1a). In turn, this field affects the nanoantenna, its dipole moment being affected only by the longitudinal (directed along the z axis, Fig. 1a) component of the electric field, created by the reflected dipole. This component can be expressed in the following form:

$$\boldsymbol{E}_{ekv} = \frac{1}{4}\frac{a^3}{z_0^3}\alpha \frac{\varepsilon_{Au} - 1}{\varepsilon_{Au} + 2}\boldsymbol{E}. \tag{2}$$

The quantity E_{ekv} can be also expressed in terms of the field of bound charges in the equivalent dielectric medium, surrounding the nanoantenna (Fig. 1b) and polarised under the action of the field E [26]:

$$\boldsymbol{E}_{ekv} = \frac{\varepsilon_{ekv} - 1}{2\varepsilon_{ekv} + 1}\boldsymbol{E}, \tag{3}$$

where ε_{ekv} is the permittivity of the equivalent medium. Equating expressions (2) and (3), one can find that the permittivity of the equivalent medium ε_{ekv} is related to the permittiv-

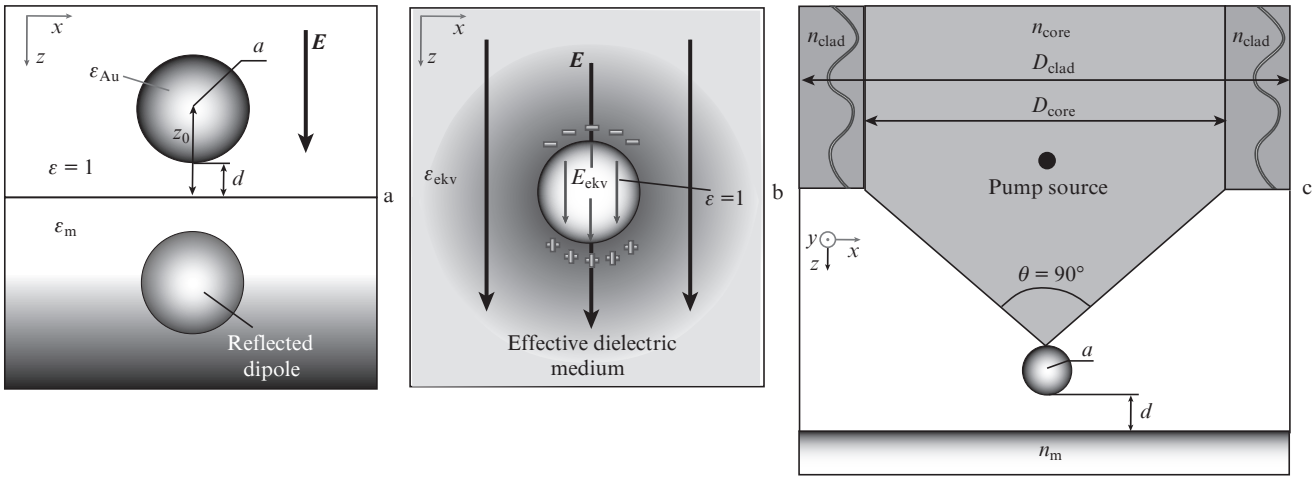

Figure 1. (a) Gold spherical nanoantenna illuminated by a plane s-polarised wave and its reflection from the semi-infinite homogeneous medium with the permittivity ε_m, placed at the distance d; (b) polarisation of the equivalent dielectric medium under the action of the uniform electric field; and (c) fibre microaxicon with the gold nanoantenna attached to its top. D_{core}, n_{core}, and D_{clad}, n_{clad} are the diameter and the refractive index of the optical core and the cladding, respectively.

ity ε_m of the semi-infinite medium placed at the distance z_0 from the nanoparticle as follows:

$$\varepsilon_{ekv} = \left[\frac{a^3(\varepsilon_m - 1)}{4z_0^3(\varepsilon_m + 1)}(\varepsilon_{Au} - 1) + (\varepsilon_{Au} + 2)\right] \times \left[4 - \frac{a^3(\varepsilon_m - 1)}{4z_0^3(\varepsilon_m + 1)}\varepsilon_{Au}\right]^{-1}. \quad (4)$$

We assume that the spectral dependence of the gold nanoparticle permittivity is described by the Drude–Lorentz relation [25]

$$\varepsilon_{Au}(\lambda) = \varepsilon_\infty - \frac{1}{\lambda_p^2(1/\lambda^2 + i/\gamma_p\lambda)}, \quad (5)$$

where ε_∞ is the permittivity in the high-frequency region; λ_p is the plasma wavelength of metal; and γ_p is the damping parameter. Neglecting the dispersion of the quantity ε_{ekv} and using the known condition for the DLPR in a small spherical nanoparticle [18]

$$\mathrm{Re}(2\varepsilon_{\varepsilon kv} + \varepsilon_{Au}) = 0 \quad (6)$$

for the case when $(\varepsilon_m - 1) \ll 1$, one can transform Eqn (4) into the expression describing the relation between the DLPR wavelength λ_{sp} of the gold spherical nanoantenna and the permittivity of the semi-infinite medium

$$\lambda_{sp} = \lambda_{sp}^{media}\sqrt{1 - \frac{(\lambda_{sp}^{media})^2 - (\lambda_{sp}^{vac})^2}{(\lambda_{sp}^{vac})^2}\left[1 - \frac{3}{4}\frac{a^3}{z_0^3}\frac{1}{(n_m^2 + 1)}\right]}, \quad (7)$$

where $n_m = \sqrt{\varepsilon_m}$; and λ_{sp}^{media} and λ_{sp}^{vac} are the DLPR wavelength values for the gold spherical nanoparticle in the homogeneous dielectric medium with ε_m and in the vacuum. The values of the latter parameters can be obtained from Eqn (5) with condition (6) taken into account. It should be noted that the values of λ_{sp}^{media} and λ_{sp}^{vac} found in this way are rather approximate, which, in turn, leads to overestimation of λ_{sp}. In this connection, for the estimation of the parameters λ_{sp}^{media} and λ_{sp}^{vac} we will use the modified Drude–Lorentz model [27], according to which

$$\varepsilon_{Au}(\lambda) = \varepsilon_\infty - \frac{1}{\lambda_p^2(1/\lambda^2 + i/\gamma_p\lambda)} + \sum_{j=1,2}\frac{A_j}{\lambda_j}\left[\frac{e^{i\varphi_j}}{(1/\lambda_j - 1/\lambda - i/\gamma_j)} + \frac{e^{-i\varphi_j}}{(1/\lambda_j + 1/\lambda + i/\gamma_j)}\right], \quad (8)$$

where the first two terms correspond to the standard Drude–Lorentz model, and the next two terms allow for the interband transitions in gold in the visible and near-IR spectral regions (λ_j is the interband transition wavelength; γ_j is the parameter allowing for the interband transition broadening; and A_j and φ_j are the dimensionless amplitude and phase of the critical points [27], respectively). Relation (8) allows the description of the gold permittivity spectral dependence in a way, providing the best correspondence to the experimentally measured values for the bulk substance [28], thus giving more accurate estimates for λ_{sp}^{media} and λ_{sp}^{vac}.

Repeating the performed calculations for the case, when the exciting field is polarised parallel to the medium surface (p-polarisation), we obtain

$$\lambda_{sp} = \lambda_{sp}^{media}\sqrt{1 - \frac{(\lambda_{sp}^{media})^2 - (\lambda_{sp}^{vac})^2}{(\lambda_{sp}^{vac})^2}\left[1 - \frac{3}{8}\frac{a^3}{z_0^3}\frac{1}{(n_m^2 + 1)}\right]}. \quad (9)$$

Figure 2 presents the dependence of the relative change in the spherical nanoparticle DLPR wavelength $\lambda_{sp}/\lambda_{sp}^{vac}$ on the RI of the semi-infinite medium [curves (*1–5*)], calculated at different distances d between the nanoparticle and the medium using expressions (7) and (9), as well as the dependence $\lambda_{sp}/\lambda_{sp}^{vac}(n_m)$ for the case, when the nanoparticle is completely surrounded by the homogeneous dielectric medium [curve (*6*)]. The latter curve is obtained using expression (8) and the condition of local dipole plasmon resonance in a small spherical nanoparticle $\mathrm{Re}(2\varepsilon_m + \varepsilon_{Au}) = 0$. As seen from the Figure, the increase in the medium RI leads to a considerable shift of the spherical nanoantenna DLPR wavelength towards the red region of the spectrum, as compared to λ_{sp}^{vac};

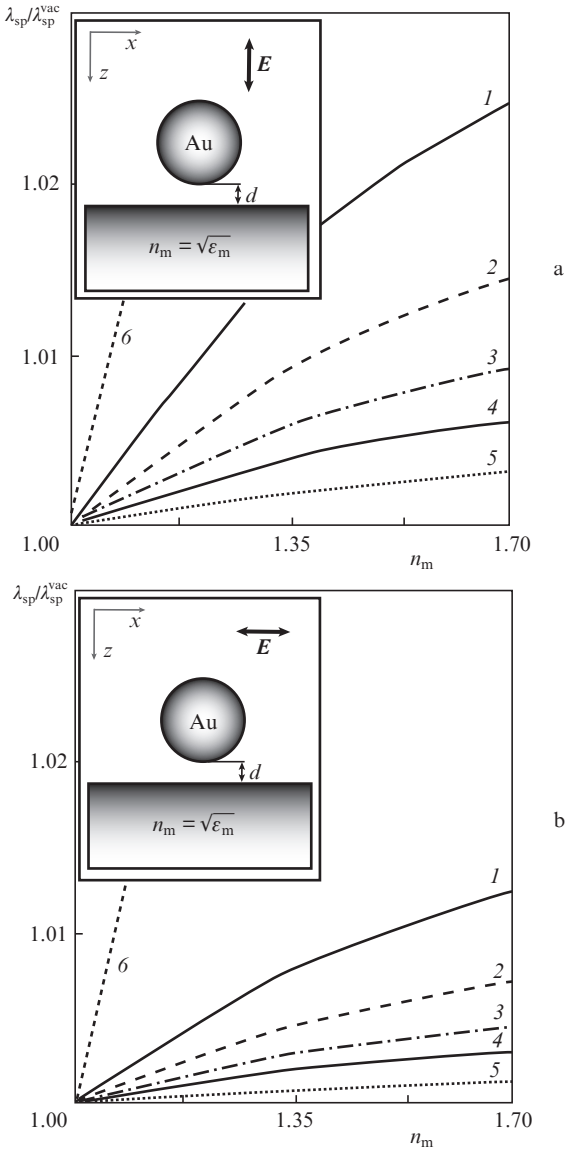

Figure 2. Dependence of the relative change in the DLPR wavelength $\lambda_{sp}/\lambda_{sp}^{vac}$ for the gold spherical nanoantenna exposed to (a) s- and (b) p-polarised external fields on the refractive index n_m of the object for d = (*1*) 0, (*2*) 10, (*3*) 20, (*4*) 30 and (*5*) 50 nm; curve (*6*) corresponds to the case, when the nanoparticle is completely surrounded by the homogeneous dielectric medium.

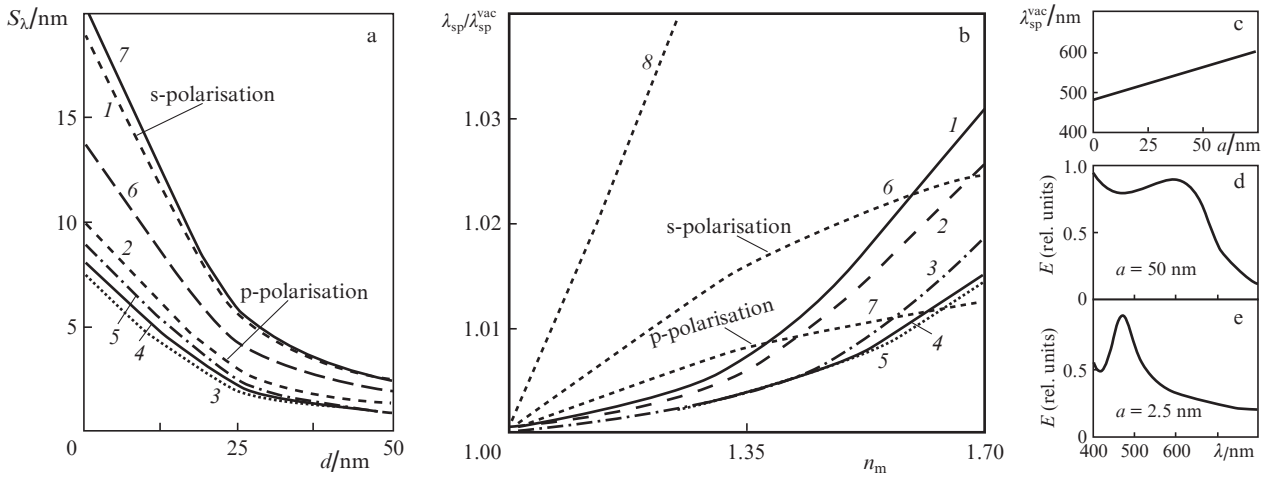

Figure 3. (a) Slope S_λ of the curve $\lambda_{sp}(n_m)$ (calculated near $n_m = 1.35$) vs. distance d, (b) relative DLPR wavelength for the spherical nanoantenna $\lambda_{sp}/\lambda_{sp}^{vac}$ vs. refractive index n_m of the semi-infinite medium and (c) DLPR wavelength λ_{sp}^{vac} of the gold nanoantenna vs. its radius a, as well as the results of calculations for the electromagnetic field strength spectrum in the near-field zone of the nanoantenna with the radius (d) 50 nm and (e) 2.5 nm; (a) curves (*1*) and (*2*) are calculated using analytic expressions (7) and (9), respectively; (*3*–*7*) are the results of numerical calculations at $a =$ (*3*) 2.5, (*4*) 6, (*5*) 12.5, (*6*) 25 and (*7*) 50 nm; (b) calculation at $d = 0$ and $a =$ (*1*) 50, (*2*) 25, (*3*) 12.5, (*4*) 6 and (*5*) 2.5 nm. Curves (*6*) and (*7*) are calculated using expressions (6) and (7), respectively; curve (*8*) corresponds to the case when the nanoantenna is completely surrounded by a homogeneous dielectric medium. The source of radiation initially placed in the axicon, produces only the p-polarised field component; however, in the focal spot at the output of the axicon the calculations carried out reveal the appearance of the s-polarised component as well.

the value of this shift being essentially dependent on the polarisation of the incident light and the distance d. It is seen that if the nanoantenna is near the surface of the semi-infinite medium [curves (*1*, *2*)], the expected spectral shift appears to be essentially smaller than when the particle is completely surrounded by the dielectric [curve (*6*)].

Figure 3a presents the slope $S_\lambda = d\lambda_{sp}/dn_m$ of the linear part of the curve $\lambda_{sp}(n_m)$, calculated near the value $n_m = 1.35$, versus the distance d [curves (*1*, *2*)]. It is seen that, as expected, the maximal spectral sensitivity $S_\lambda \sim 19$ nm is attained in the case of the s-polarised exciting field and $d = 0$, which is obviously explained by the character of the distribution of energy density maxima in the near-field zone of the dipole nanoantenna radiation [29, 30]. Note that S_λ is only 4 times smaller than the sensitivity of the nanoantenna, completely surrounded by the dielectric. With the resolution of up-to-date optical spectrum analysers, evaluated in correspondence with the Rayleigh criterion (no worse than 0.02 nm) [31] taken into account, the proposed method can provide the possibility to detect the RI changes of $\sim 10^{-3}$. However, keeping in mind the existing methods of optical spectrum processing, based on the detection of the 'centre of gravity' of a spectral peak [32], one can expect an increase in the limiting resolution of the developed method at least by an order of magnitude (to $\sim 10^{-4}$).

3. Numerical modelling

As mentioned above, to provide the possibility of mapping the small variations in the studied object RI under real experimental conditions, the nanoantenna should be placed at the tip of the scanning probe, be able to focus the optical radiation efficiently on the nanoantenna surface with minimal background exposure of the studied object and also be incorporated in the feedback system of a standard probe microscope, thereby providing the possibility of precise movement of the nanoantenna near the surface of the studied object. Let us assume that the nanoantenna is placed at the top of the fibre microaxicon (FMA) (see Fig. 1c), formed at the face of an optical fibre. The nanoantenna is separated by the distance d from the boundary of the semi-infinite dielectric medium with the refractive index n_m, varying from 1 to 1.7. The presence of the axicon causes a certain difference of the considered geometry from the conditions, underlying the analytic model. It is also worth noting that the quasi-static approximation described above can be considered valid only in the case of a spherical nanoantenna having the relatively small radius a (i.e., for $a < \sigma$, where σ is the skin layer thickness for gold). To take the delay of electron density field oscillations inside the nanoantenna [30] with $a > \sigma$ into account and to estimate the possible influence of the microaxicon, to which the nanosphere is attached, on the spectral sensitivity of the method, we perform the numerical modelling using the time-domain finite-difference method [33]. It is also assumed that the FMA has the convergence angle $\theta = 90°$, the base diameter, equal to that of the core of the optical fibre, and possesses axial symmetry with respect to the optical axis of the fibre (the z axis in Fig. 1c). In correspondence with the data of Ref. [34], such geometric parameters of the axicon provide focusing of the laser radiation launched into the fibre, into a diffraction-limited spot with the lateral size $\sim\lambda/2$ and the focal length $\sim 0.3\lambda$, which can provide high efficiency of the DLPR excitation in the nanoantenna with minimal background exposure. For modelling the optical properties of the fibre, the following parameters are used: the core diameter $D_{core} = 4.5$ μm, the cladding diameter $D_{clad} = 125$ μm, and the numerical aperture NA = 0.14. The FMA is excited with the broadband p-polarised Gaussian radiation source (its position is shown in Fig. 1c) with the centre wavelength $\lambda_c = 532$ nm and the spectral half-width $\Delta\lambda_{FWHM} = 100$ nm. With the parameters indicated above in the considered spectral range a single-mode regime of the optical radiation propagation is implemented in the fibre [35]. Perfectly matched layers are used as the boundaries for the calculation domain. The mesh of the calculation grid has the dimensions $1\times1\times1$ nm. Besides, to increase the accuracy of calculations in the nanoantenna region the additional grid is used with the mesh size $0.2\times0.2\times0.2$ nm.

Figure 3b presents the dependences of the relative DLPR wavelength of the spherical nanoantenna $\lambda_{sp}/\lambda_{sp}^{vac}$ on the RI n_m of the semi-infinite medium, calculated for different a and $d = 0$ [curves (*1–3*)]. As shown by the results of calculations, for small ($a < 25$ nm) radii the quantity λ_{sp}^{vac} is not constant and linearly grows with the growth of the nanoantenna radius (Fig. 3c), which also agrees with the data of Refs [29, 30]. Therefore, for the convenience of presenting the dependences calculated numerically and analytically, the quantity λ_{sp} in each case is normalised to the DLPR wavelength λ_{sp}^{vac}, corresponding to the particular radius of the nanoantenna, a. For comparison Fig. 3b shows the results of calculations of the dependence $\lambda_{sp}/\lambda_{sp}^{vac}(n_m)$, obtained using the analytic model for s- and p-polarised radiation [curves (*6*) and (*7*), respectively], and also the analytic dependence $\lambda_{sp}/\lambda_{sp}^{vac}(n_m)$, corresponding to the case, when the nanoparticle is completely surrounded by the homogeneous dielectric medium [curve (*8*)].

It is seen that for small-radius nanoantennas [curves (*3–5*)] the value of the relative spectral shift $\lambda_{sp}/\lambda_{sp}^{vac}$, evaluated using the numerical calculations, is in good agreement with the results, obtained on the basis of the analytic model [curves (*6*, *7*)]. In the region of small refractive indices ($1 < n_m < 1.3$) the curves, calculated both numerically and analytically, demonstrate a virtually linear growth of $\lambda_{sp}/\lambda_{sp}^{vac}$ with increasing n_m. However, the value of $\lambda_{sp}/\lambda_{sp}^{vac}$ for all numerically calculated curves appears to be somewhat greater than that evaluated using expression (7) for the case of the nanoantenna illumination with p-polarised radiation. This fact can be partially explained by the presence of a longitudinal field component, directed along the z axis, in the focal spot of the FMA. Moreover, the analysis of the data presented in Fig. 3b shows a tendency towards the slope S_λ increase with the growth of n_m, mutual for all numerically calculated curves, whereas the slope of the dependence $\lambda_{sp}/\lambda_{sp}^{vac}(n_m)$, obtained using the analytic expressions (7) and (9), decreases with increasing n_m. The disagreement of the results obtained numerically and analytically is explained by the fact that the assumption $(\varepsilon_m - 1) \ll 1$ made in the analytic model becomes invalid in the considered range of n_m values. Besides, for obtaining a more precise analytic model it seems necessary also to allow for the influence of multiple reflections of the equivalent dipole and nanoantenna, the contribution of which increases with increasing medium RI.

Figure 3a presents the results of the numerical calculations of the dependence of S_λ on the distance d [curves (*3–7*)]. It is seen that in spite of a certain disagreement in the estimates of the maximal values of S_λ for $d = 0$, the behaviour of the curves demonstrates good correspondence with the results of the analytic model [curves (*1*, *2*)]. It should be also noted that the dependences $S_\lambda(d)$ for nanoantennas with the radius exceeding the skin layer thickness [curves (*6*, *7*) in Fig. 3a] almost coincide both with the results of the numerical calculations for the nanoantenna radius $a < \sigma$ [curves (*3–5*)] and with the analytically calculated curves (*1*) and (*2*). However, with an increase in a [curves (*1*, *2*) in Fig. 3b], the slope of the dependence $\lambda_{sp}/\lambda_{sp}^{vac}(n_m)$ increases, and for $a > 25$ nm the value of S_λ exceeds the one, obtained using expression (9), and attains the maximal value ~21 nm at $a = 50$ nm. Such a growth of the slope of the curves with increasing a is, apparently, explained by the effect of delay of the electron density oscillations in the nanoantenna, which was also reported in Ref. [31]. Besides that, with the growth of the nanoantenna radius a, the spectral half-width of the DLPR (Figs 3d and 3e) strongly increases, which is potentially able to hamper the detection of the spectral shift (the analogous results were demonstrated in Ref. [29]). The lateral resolution in the process of the RI distribution profile scanning becomes worse with the growth of the nanoantenna size. Apparently, this can reduce the positive effect of using the nanoantennas with large radius. In our opinion, the use of nanoantennas with $a < 50$ nm is optimal from the point of view of the balance between the lateral resolution and the sensitivity of the RI registration (no worse than 5×10^{-4}).

4. Conclusions

Thus, within the framework of the present paper we have theoretically shown that the use of the spectral response of a single spherical gold nanoantenna allows detection of extremely small (to 5×10^{-4}) variations in the refractive index of the studied object surface. Using the quasi-static approximation we have developed the analytic model that allows the spectral shift of the nanoantenna DLPR to be estimated. The point probe on the basis of a fibre microaxicon with a gold spherical nanoantenna attached to its top is proposed that allows implementation of the developed RI scanning method. The results of numerical calculations of the probe characteristics using the time-domain finite-difference method are presented, and it is shown that for a nanoantenna having small size comparable with the gold skin layer thickness the value of the relative DLPR spectral shift is in good agreement with the results obtained from the analytic model developed. The technology of fibre microaxicon fabrication is developed sufficiently well. The nanoantenna at the top of the microaxicon can be fabricated using several experimental techniques, such as ion beam lithography, direct transfer of nanoparticles under the action of femtosecond laser pulses [36], or scanning single gold particles [37]. The excitation and recording of the nanoantenna DLPR spectral shift using the proposed point probe on the basis of FMA with a nanoantenna attached to its top can be implemented both in the regime of lateral illumination and with the illumination directly through the probe that potentially allows essential simplification of the optical radiation collection system. The experimental implementation of the described probe for mapping small variations in the RI of the studied object surface, as well as the numerical and experimental estimates of the lateral resolution, will be demonstrated in our next paper.

Acknowledgements. The work was partially supported by the Russian Foundation for Basic research (Grant Nos 14-02-31323_mol_a, 13-02-00648-a, 14-02-00205-a) and Programme No. 24 of the Presidium of the Russian Academy of Sciences.

References

1. Huber A.J., Kazantsev D., Keilmann F., Wittborn J., Hillenbrand R. *Adv. Mater*., **19**, 2209 (2007).
2. Vogel E.M. *Nat. Nanotech*., **2**, 25 (2007).
3. Taubner T., Hillenbrand R., Keilmann F. *Appl. Phys. Lett.*, **85**, 5064 (2004).
4. Vobornik D., Margaritondo G., Sanghera J.S., Thielen P., Aggarwal I.D., Inanov B., Tolk N.H., Manni V., Grimaldi S., Lisi A., Rieti S., Piston D.W., Generosi R., Luce M., Perfetti P., Cricenti A. *J. Alloys Compd*., **401**, 80 (2005).
5. Bharadwaj P., Deutsch B., Novotny L. *Adv. Opt. Photon*., **1**, 438 (2009).
6. Rayleigh L. *Phil. Mag.*, **8**, 261 (1879).
7. Novotny L., van Hulst N.F. *Nat. Photon*., **5**, 83 (2011).
8. Novotny L., Bian R.X., Xie X.S. *Phys. Rev. Lett*., **79**, 645 (1997).

9. Sundaramurthy A., Schuck P.J., Conley N.R., Fromm D.P., Moerner W.E., Kino G.S. *Nano Lett.*, **6**, 355 (2006).
10. Frey G.F., Witt S., Felderer K., Guckenberger R. *Phys. Rev. Lett*., **93**, 200801 (2004).
11. Betzig E., Chichester R.J. *Science*, **262**, 1422 (1993).
12. Taubner T., Hillenbrand R., Keilmann F. *J. Microsc.*, **210**, 311 (2003).
13. Taubner T., Keilmann F., Hillenbrand R. *Opt. Express*, **13**, 8893 (2005).
14. Sanchez E.J., Novotny L., Xie X.S. *Phys. Rev. Lett*., **82**, 4014 (1999).
15. Gerton J.M., Wade L.A., Lessard G.A., Ma Z., Quake S.R. *Phys. Rev. Lett*., **93**, 180801 (2004).
16. Taminiau T.H., Moerland R.J., Segerink F.B., Kuipers L., van Hulst N.F. *Nano Lett.*, **7**, 28 (2007).
17. Veerman J.A., Otter A.M., Kuipers L., van Hulst N.F. *Appl. Phys. Lett.*, **72**, 3115 (1998).
18. Novotny L., Hecht B. *Principles of Nano-Optics* (Cambridge: Cambridge Univ. Press, 2006).
19. Farahni J.N., Pohl D.W., Eisler H.-J., Hecht B. *Phys. Rev. Lett*., **95**, 017402 (2005).
20. Sendur K., Challener W., Peng C. *J. Appl. Phys*., **96**, 2743 (2004).
21. Lee T., Lee E., Oh S., Hahn J.W. *Nanotechnol.*, **24**, 145502 (2013).
22. Kulchin Yu.N., Vitrik O.B., Bezverbnyi A.V., Pustovalov E.V., Kuchmizhak A.A., Nepomnyashchii A.V. *Kvantovaya Elektron*., **41**, 249 (2011) [*Quantum Electron*., **41**, 249 (2011)].
23. Kulchin Yu.N., Vitrik O.B., Kuchmizhak A.A., Pustovalov E.V., Nepomnyashchii A.V. *Opt. Lett.*, **36**, 3945 (2011).
24. Lee K.-S., El-Sayed M.-A. *J. Phys. Chem. B*, **110**, 19220 (2006).
25. Born M., Wolf E. *The Principles of Optics* (Oxford: Pergamon Press, 1964).
26. Matveev A.N. *Elektrichestvo i magnetism* (Electricity and Magnetism) (Moscow: Vysshaya Shkola, 1983).
27. Etchegoin P.G., Le Ru E.C., Meyer M. *J. Chem. Phys*., **125**, 164705 (2006).
28. Johnson P.B., Christy R.W. *Phys. Rev. B*, **6**, 4370 (1972).
29. Kelly K.L., Coronado E., Zhao L.L., Schatz G.C. *J. Phys. Chem. B*, **107**, 668 (2003).
30. Bryant G.W., García de Abajo F.J., Aizpurua J. *Nano Lett.*, **8**, 631 (2008).
31. www.yokogawa.com.
32. Kulchin Yu.N., Vitrik O.B., Kuchmizhak A.A. *J. Opt. Soc. Am. B*, **30**, 598 (2013).
33. Taflove A., Hagness S.C. *Computational Electrodynamics: The Finite-Difference Time-Domain Method* (London: Artech House Inc., 2000).
34. Kuchmizhak A.A., Gurbatov S.O., Nepomniaschii A.A., Vitrik O.B., Kulchin Yu.N. *Appl. Opt*., **53**, 937 (2014).
35. www.thorlabs.com.
36. Kuznetsov A.I., Evlyukhin A.B., Gonçalves M.R., Reinhardt C., Koroleva A., Arnedillo M.l., Kiyan R., Marti O., Chichkov B.N. *ASC Nano*, **5**, 4843 (2011).
37. Anger P., Bharadwaj P. Novotny L. *Phys. Rev. Lett*., **96**, 113002 (2006).